Jet-cooled laser spectroscopy and solid-state vibrational circular dichroism of the cyclo-(Tyr-Phe) diketopiperazine dipeptide

Jennifer Dupont, Régis Guillot, Valéria Lepère, Anne Zehnacker

Journal of Molecular Structure xxx (xxxx) 133059

Contents lists available at ScienceDirect

Journal of Molecular Structure

journal homepage: www.elsevier.com/locate/molstruc

Jet-cooled laser spectroscopy and solid-state vibrational circular dichroism of the cycloTyr-Phe-diketopiperazine dipeptide

Jennifer Dupont [a], Régis Guillot [b], Valéria Lepère [a], Anne Zehnacker [a, *]

[a] Institut des Sciences Moléculaires d'Orsay (ISMO), CNRS, Université Paris-Saclay, F-91405 Orsay, France
[b] Université Paris-Saclay, CNRS, Institut de Chimie Moléculaire et des Matériaux d'Orsay (ICMMO), 91405 Orsay, France

ARTICLE INFO

Article history:
Received 16 February 2022
Received in revised form 9 April 2022
Accepted 9 April 2022

Keywords:
Diketopiperazine
Laser spectroscopy
Vibrational circular dichroism
Tyrosine
Phenylalanine
Supersonic expansion

ABSTRACT

The structures of the diastereomer diketopiperazine dipeptides cycloLTyr-LPhe and cycloDTyr-LPhe are studied in the gas phase using resonance-enhanced two-photon ionization, IR/UV double resonance spectroscopy and quantum chemical calculation. Both diastereomers exhibit two conformations, with the tyrosine ring folded over the DKP ring and the phenylalanine ring extended outwards, or *vice versa*. The two diastereomers differ only slightly by the nature of weak CH•••π and NH•••π interactions. The crystal structure of cycloLTyr-LPhe is determined by X-ray crystallography and is composed of monomers with folded tyrosine ring. The vibrational circular dichroism spectrum is interpreted by the existence of dimers in the solid state. Quantum chemical calculation shed light on the structural modifications between the gas phase and the solid state.

1. Introduction

Diketopiperazines (DKPs) are cyclic dipeptides formed by condensation of two α-amino acids. They are ubiquitous in nature and may be found as degradation products of processed food and beverages, in particular those containing artificial sweeteners. Due to their H-bond donor and acceptor ability, the DKPs can bind to a wide range of receptors and thus are attractive scaffolds for drug discovery [1]. In particular, cycloDTyr-DPhe based on tyrosine (Tyr) and phenylalanine (Phe) was isolated from *Bacillus* bacteria and shows an antibacterial, anticancer and antioxidant activity. However, cycloLTyr-LPhe was found to be less bioactive than its enantiomer [2]. This might be due to its smaller resistance to proteolysis, specific to the L-amino acids. Indeed, although D-amino acids can be found in bacteria or antibiotics, only the L-amino acids polymerize to form proteins in the living organisms. The origin of the homochirality of life is still an unresolved issue.

We have recently studied the effect of chirality on the structure of jet-cooled cycloTyr-Pro, [3] cycloPhe-Phe [4] and cycloTyr-Tyr [5] with conformer-selective vibrational spectroscopy and quantum chemical calculations. Two conformations are experimentally observed for the cycloTyr-Pro-diastereomers, the most stable one with the phenol ring folded over the DKP ring and the other one with the phenol ring extended. The cycloTyr-Pro-diastereomers only differ from each other by the nature of the CH•••π interaction in the folded conformer and in the strength of the NH•••π interaction in the extended conformer. Cyclo Phe-Phe-and cycloTyr-Tyr-contain two identical flexible residues. Their most stable conformation shows one of the aromatic rings folded over the DKP ring and the other one extended outwards. This structure has been confirmed for cycloPhe-Phe-by IR-UV experiments in the far IR range [6]. Chirality effects stem from the nature of the carbon atom involved in the CH•••π interaction, namely C_α or C_β, and the strength of the NH•••π interaction. Cyclo LTyr-LTyr stands out by the stabilization of an additional conformation with the two aromatic rings parallel to each other. In this staked conformation, the repulsion between the two aromatic rings is counterbalanced by the formation of an OH•••O hydrogen bond between the phenol rings. This conformation is not observed in cycloLPhe-LPhe where repulsion prevails and cannot be counterbalanced by the sole dispersion. Because of the steric constraints, such an OH•••O hydrogen bond cannot exist in cycloLTyr-DTyr, resulting in strong chirality effects on the structure of cycloTyr-Tyr. Here, we extend this study to cycloTyr-Phe, shown in Fig. 1. This system possesses two chromophores, like cyclo Phe-Phe-and cycloTyr-Tyr, but it is asymmetrically substituted, which can enrich its conformational landscape. We chose this system to assess whether the stacked geometry was

* Corresponding author.
E-mail address: anne.zehnacker-rentien@universite-paris-saclay.fr (A. Zehnacker).

https://doi.org/10.1016/j.molstruc.2022.133059
0022-2860/© 20XX

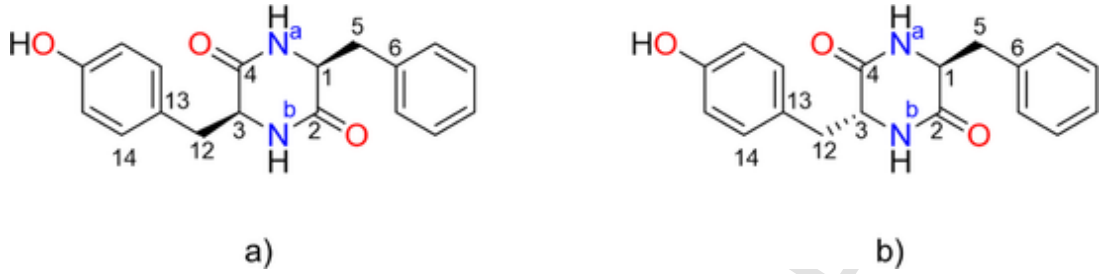

Fig. 1. Structure of cycloTyr-Phe-and atom numbering. a) Homochiral dipeptide c-LL b) Heterochiral dipeptide c-DL.

stable for cycloLTyr-LPhe thanks to a possible OH•••π interaction. Strickland et al. studied cycloLTyr-LPhe by electronic circular dichroism and proposed that the stacked conformation was the most stable one in an ethyl ether – isopentane – ethanol (EPA) mixture and in methanol [7]. Later, Yamazaki et al. studied cycloLTyr-LPhe and cycloLTyr-DPhe in DMSO-d_6 using ^{1}H NMR spectroscopy and molecular mechanics. They came to the same conclusion that the stacked conformation of cycloLTyr-LPhe was predominant and the most stable structure according to the force field calculations. For cycloLTyr-DPhe, two stacked conformations were observed in DMSO-d_6, for which the two rings are folded over the DKP ring, from opposite sides [8]. The two studies mentioned above use strongly polar or protic solvents, which might considerably modify the conformation of the studied molecule. In this work, the two diastereomers of cycloTyr-Phe, namely, c-LL and c-DL, are studied under jet-cooled conditions, thus without the possible solvent-induced perturbation. In addition, vibrational circular dichroism experiments shed light on the structure of c-LL in the solid state. Vibrational circular dichroism is indeed a powerful technique for the structural study of peptides, both in the liquid [9–11] and in the solid state [12] [13–15].

2. Experimental and theoretical methods

The cyclic dipeptides cycloTyr-Phe (99%) were purchased from Novopep Limited (Shanghai – China) and used without further purification.

2.1. Gas phase spectroscopy

The pulsed supersonic beam was produced by expanding argon (~ 4 bar) seeded with the molecule under study into a vacuum chamber (~ 10^{-6} mbar) through a 200 µm pulsed nozzle (General Valve - Parker) [16]. The dipeptides were put into the gas phase thanks to a homemade laser desorption source [17]. The second harmonic of a Nd:YAG laser (Continuum Minilite) was propagated by an optical fiber to the surface of a 5 cm long graphite bar, spread with a few mg of the dipeptide under study. The graphite bar was fixed on a linear translation system to continuously irradiate a fresh area, so that the same bar could be used continuously for one or two days. The supersonic expansion intercepted the produced plume at the output of the valve.

Mass-resolved S_0-S_1 spectra were obtained using one-color resonance-enhanced two-photon ionization (RE2PI) spectroscopy. The UV source (0.02 cm^{-1} resolution) was generated by doubling the output of a dye laser (Sirah equipped with C540A dye) pumped by the second harmonic of a Nd:YAG laser (Quanta Ray, Spectra Physics). The UV laser beam was gently focused (focal length of 1 m) in the interaction region of a linear time-of-flight (TOF) mass spectrometer (Jordan, one-meter length), where it crossed the supersonic beam. The formed ions were detected by a microchannel plate detector (RM Jordan, 25 mm diameter). The ion signal was averaged by an oscilloscope (Lecroy wavesurfer) and processed through a personal computer.

Vibrational spectra were recorded using the IR-UV double resonance method [18, 19]. An IR laser beam (3 cm^{-1} resolution) was counterpropagated relative to the UV laser beam and was mildly focused (focal length of 0.5 m) in the interaction region of the TOF. The UV probe laser was fixed on each main vibronic transition detected in the S_0-S_1 spectrum, and the wavelength of the IR pump laser was scanned in the region of 3 µm, so that the IR absorption was detected as a dip in the UV-induced ion signal. The IR source was an optical parametric oscillator/amplifier (OPO/OPA) (Laser Vision). The IR pulse was triggered 80 ns before the UV pulse to record ground state vibrational spectra and 40 ns afterwards to record vibrational spectra of the ions. Synchronization between the lasers was controlled by a homemade gate generator. The IR spectra were recorded with an active baseline scheme, by measuring the difference in ion signal produced by successive UV laser pulses (one without and one with the IR laser pulse) [20].

2.2. IR spectroscopy and VCD in the solid state

The vibrational IR absorption and VCD spectra in the solid state were measured using a FTIR spectrometer (Vertex 70 Bruker) equipped with a VCD module (PMA 50 Bruker). The signal was measured by a MCT IR detector with a BaF_2 window, cooled with liquid nitrogen. A spectral resolution of 4 cm^{-1} was used for both absorption and VCD spectra. The IR radiation was polarized with a linear polarizer then modulated by a 50 kHz ZnSe photoelastic modulator (Hinds Instruments). A low-pass filter cutting at 2000 cm^{-1} was added before the linear polarizer to increase the dynamic response of the detector. The signal of the MCT detector was demodulated using a lock-in amplifier (Stanford Research Systems SR 830). 5 mg of the dipeptide under study were first grinded with 3 g of oven-dried (80 °C) KBr in a mixer mill (MM 400, Retsch) at 20 Hz for 1 h, to obtain a homogeneous mixture and decrease the size of the microcrystals down to 10 µm in diameter. This procedure allows minimizing spurious signals due to scattering and birefringence. Thin pellets were made with 150 mg of this mixture using a hydraulic press, under approximatively 3.5 tons for 5 min, and then gently heated to 80 °C to eliminate most of the water. The concentration in dipeptides and the thickness of the pellet were defined to limit the optical density of the most intense bands to 0.8, which is a necessary condition for obtaining reliable VCD spectra [21, 22]. The artifacts due to the KBr pellets birefringence were corrected by following the procedure proposed by Merten et al., [23] derived from that introduced by Buffeteau et al. [24] It consists in rotating the sample in the plane perpendicular to the light propagation axis for each side (front and back) of the pellet and averaging the spectra obtained for the 0° and 90° positions. To have a better average, the procedure was extended to 180° and 270°. The acquisition time was 30 min for each position. The VCD spectra presented here are the half difference of the VCD spectra of c-LL and c-DD; the raw data are presented in the SI section.

2.3. Crystallography

The c-LL crystals were grown from a saturated solution in ethanol prepared at a temperature slightly below the solvent boiling point and then allowed to slowly cool down. X-ray diffraction data were collected using a VENTURE PHOTON100 CMOS Bruker diffractometer with Mi-

cro-focus IuS source Cu Kα. The crystals were mounted on a CryoLoop (Hampton Research) with Paratone-N (Hampton Research) as cryoprotectant and then flash frozen in a nitrogen-gas stream at 100 K. For all compounds, the temperature of the crystal was maintained at the selected value by means of a 700+ series Cryostream cooling device within an accuracy of ±1 K. The data were corrected for Lorentz polarization, and absorption effects. The structures were solved by direct methods using SHELXS-97 [25] and refined against F^2 by full-matrix least-squares techniques using SHELXL-2018 with anisotropic displacement parameters for all non-hydrogen atoms [26]. Hydrogen atoms were located on a difference Fourier map and introduced into the calculations as a riding model with isotropic thermal parameters. All calculations were performed by using the Crystal Structure crystallographic software package WINGX [27].

The crystal data collection and refinement parameters are given in Table S1 of the Supporting Information (SI).

2.4. Theoretical methods

Gas phase structure and IR spectra: Geometry optimization and vibrational frequencies calculation were performed with the Gaussian Package (Version 16 Rev. B.01), [28] using the B3LYP functional combined to the 6-311++G(d,p) basis set, [29] and including D3 empirical corrections for dispersion [30, 31]. D3 dispersion corrections were preferred to more recent versions to facilitate the comparison with previously studied systems, namely cycloPhe-Phe, cycloTyr-Tyr-and cyclo-Tyr-Pro [3-5, 32]. The local minima of the potential energy surfaces (PES) of cycloLTyr-LTyr and cycloLTyr-DTyr monomers were used as starting structures for the geometry optimizations, with an H atom in place of one of the OH groups [5].

The vibrational frequencies were calculated in the frame of the harmonic approximation at the same level of theory and the absence of imaginary frequencies was checked for all local minima. The obtained harmonic frequencies were multiplied by a scaling factor of 0.952 to compensate for anharmonicity and basis set incompleteness [5, 33]. The spectra were simulated by convoluting the scaled frequencies by a Lorentzian line shape of 4 cm^{-1} full width at half maxima (FWHM). Gibbs free energies ΔG relative to the most stable conformation were computed at 298.15 K, thus yielding the Boltzmann populations prior to the expansion. The charge distribution was obtained from the Natural Bond Orbital (NBO) analysis [34].

The parameters chosen to describe the cycloTyr-Phe-geometry are the same as used previously for cycloTyr-Tyr-or cycloPhe-Phe-and are detailed in Fig. 2. For each aromatic ring, three orientations are possible: g^+, g^- (gauche geometries) and t (trans). These orientations correspond to dihedral angles $\tau(N_a\ C_1\ C_5\ C_6)$ (for the phenylalanine ring) or $\tau(N_b\ C_3\ C_{12}\ C_{13})$ (for the tyrosine ring) of around 60°, −60° and 180°, respectively, for the L residue, while the angles for the D residue are of opposite sign. The different monomer conformations will be named c-Tyr(g^+, g^- or t; L or D)-Phe(g^+, g^- or t; L). Moreover, two orientations I and II of the OH bond of tyrosine for each conformation are possible. As already observed for dipeptides containing tyrosine as well as tyrosine itself, the conformers corresponding to the two orientations cannot be distinguished by their IR spectra [3, 5, 35-38]. We will therefore think in terms of "families" including both orientations of the OH bond, except when specified otherwise.

IR and Vibrational circular dichroism in the solid phase: Calculation of VCD spectra in the solid state is hampered by difficulties related to the infinite nature of the crystal [39]. Although non-local effects are important for calculating VCD intensities, [40, 41] approaches considering clusters of limited size can be used for obtaining reliable simulated VCD spectra [15, 42-44]. We use the very same approach here, starting from clusters of different sizes, whose geometry is deduced from the crystal structure with modification of the side chain arrangement, if necessary (*vide infra*). The VCD intensities were calculated using the Magnetic Field Perturbation Theory (MFPT) implemented in the Gaussian software [45, 46]. The IR and VCD spectra were calculated at the B3LYP-D3/6-31G(d,p) level and the spectra simulated by convoluting the harmonic frequencies scaled by 0.940 with a Lorentzian of 8 cm^{-1} FWHM.

3. Results and discussion

3.1. Gas phase results

3.1.1. Calculated structures

Ground state S_0: The most stable calculated structures of c-LL are shown in Fig. 3(a). Only one member of the family is shown for conformers differing only in the orientation of the OH bond and separated by less than 0.2 kcal.mol^{-1}. More details about the optimized structures can be found in Table S2 of the SI. The most stable group of conformers is c-Tyr(g^+_L)-Phe(g^-_L), in which the tyrosine ring is folded over the DKP ring and the phenylalanine ring is extended. The second most stable group is c-Tyr(g^-_L)-Phe(g^+_L), in which the roles of the phenylalanine and the tyrosine rings are inverted. Both families are stabilized through weak $C_\beta H\bullet\bullet\bullet\pi$ and $NH\bullet\bullet\bullet\pi$ interactions. While these two groups are almost isoenergetic, c-Tyr(g^-_L)-Phe(g^-_L) where both rings are extended is 1.7 kcal.mol^{-1} higher in energy than the most stable form. This family involves two weak $NH\bullet\bullet\bullet\pi$ interactions. The c-Tyr(g^+_{LL})-Phe(g^+_L) conformers, which have their phenyl rings in a stacked position, are more than 2.5 kcal.mol^{-1} higher in energy than the most stable form. They stand out by the fact that the Gibbs free energy difference between c-Tyr(g^+_{LL})-Phe(g^+_L) and c-Tyr(g^+_{LII})-Phe(g^+_L) is no-

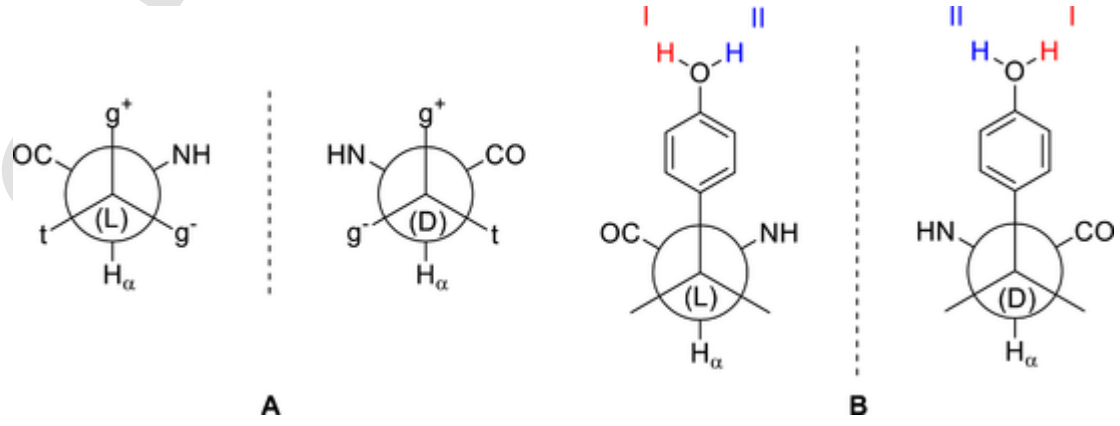

Fig. 2. (A) Aromatic ring positions corresponding to g^+, g^- (gauche) and t (trans) geometries for the L (left) and D (right) absolute configurations of the stereogenic centers. (B) Orientations I (in red) and II (in blue) of the phenol hydroxyl for L and D tyrosine, which can exist for each position g^+, g^- and t of the phenol ring.

ticeable (0.4 kcal.mol^{-1}). Non Covalent Interaction (NCI) calculations [47, 48] (not shown) suggest that this difference is due to a weak $C_{arom}H\bullet\bullet\bullet O$ interaction possible in the former that cannot be formed in the latter structure. The destabilization of the stacked conformer contrasts with what was observed in cycloTyr-Tyr-where it was destabilized by only 0.2 kcal.mol^{-1} relative to the most stable form thanks to a hydrogen bond between the two hydroxyl groups [5]. Here, c-Tyr(g^+_L)-Phe(g^+_L) does not display the expected OH•••π(Phe) interaction which could have stabilized the structure. To check that such a local minimum has not been missed in the calculations, a relaxed potential energy surface scan was performed starting from c-Tyr(g^+_{LL})-Phe(g_L). The dihedral angle τ(C_3 C_{12} C_{13} C_{14}) was varied from 82° to 442° by 5° increments. The corresponding relaxed scan is displayed in Fig. S1 of the SI. It shows only the two previously found local minima c-Tyr(g^+_{LL})-Phe(g_L) and c-Tyr(g^+_{LII})-Phe(g^+_L). Indeed, dispersion between the two aromatic rings is optimal in those structures. Rotating the tyrosyl ring decreases the contribution of dispersion and steric hindrance prevents the formation of an OH•••π(Phe) interaction. Then, only the first two families of conformations are expected to be observed under supersonic expansion conditions. These results are very similar to what was observed in cycloPhe-Phe, for which the only stable structure has one of the aromatic ring folded over the DKP ring and the other one extended [4, 6]. However, these results disagree with those of Yamazaki. [8] This disagreement may be explained by the presence of the DMSO solvent which can disrupt the intramolecular bonds [49] and by the deficiency of the force fields used at the time of his work. The most stable calculated structures of c-DL are shown in Fig. 3b. The structural parameters and the energetics are listed in Table S3 of the SI. The relative energies of the different conformational families are the same as for c-LL. The two most stable families of c-DL, namely c-Tyr(g^+_D)-Phe(g^-_L) and c-Tyr(g^-_D)-Phe(g^+_L), parallel those of c-LL, with one ring folded and the other one extended. It should be noted that the most stable c-DL conformer is 0.53 kcal.mol^{-1} higher in energy than the most stable c-LL conformer, which shows an energetic homochiral preference. Similar conclusions were drawn for neutral cycloPhe-Phe-and cycloTyr-Tyr [3, 5, 32] or protonated cycloPhe-Phe-and cycloHis-Phe, [50, 51] which points to a homochiral energetic preference. c-DL differs from c-LL by the presence of an extra conformation below 3.0 kcal.mol^{-1}, c-Tyr(g^+_{DII})-Phe(t_L), with a folded tyrosine aromatic ring and the extended phenylalanine ring undergoing a rotation of 120° compared to c-Tyr(g^+_D)-Phe(g^-_L). As frequently observed in diastereomer peptides studied so far, whether linear or cyclic, [4, 5, 50-52] more conformations are calculated in a low energy window for c-DL than c-LL, which points to the larger flexibility of the heterochiral peptide.

The two most stable families of c-DL are stabilized by NH•••π and C_αH•••π interactions. The nature of the carbon atom involved in the CH•••π interaction is the main difference between the two diastereomers c-LL and c-DL. Because of stereochemical constraints, the CH donor group cannot be the same in both diastereomers, as already observed in cycloPhe-Phe-and cycloTyr-Tyr [3, 5, 32]. The c-Tyr(g^+_D)-Phe(g^+_L) conformation is calculated 1.4 kcal.mol^{-1} higher in energy than the most stable form, which contrasts with the results of Yamazaki et al., who suggested that this sandwich structure was the most stable form in DMSO [8]. Besides, c-Tyr(g^+_{DII})-Phe(t_L) is 0.6 kcal.mol^{-1} more stable than c-Tyr(g^+_{DI})-Phe(t_L), because the OH bond is not exactly coplanar with the aromatic ring and tends to interact with the phenylalanine ring through a weak OH•••π interaction (shown by the NCI calculations). However this structure is not very stable due to the lack of NH•••π interaction.

For c-LL and c-DL alike, two families of conformers are therefore expected to be populated hence experimentally detected.

Ionic state D_0: The local minima of the cation were obtained by removing one electron from the local minima of the neutral form and by optimizing the resulting cation. The energetics of the optimized structures are listed in Table S4 of the SI. The most stable families of the c-LL cation are displayed in Fig. 4. c-Tyr(t_L)-Phe(g^+_L) where the tyrosine ring is extended and the phenylalanine is folded is the most stable

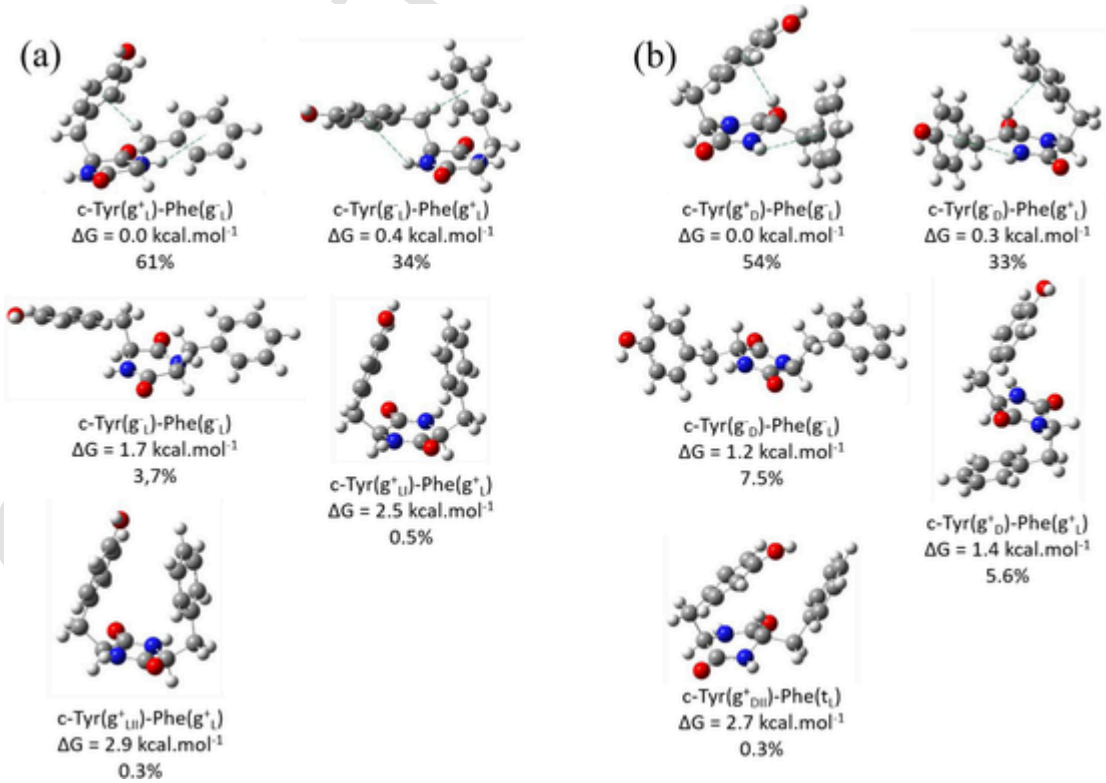

Fig. 3. Most stable calculated structures (ΔG < 3.0 kcal.mol^{-1}) of c-LL (a) and c-DL (b) with their Boltzmann populations. Only the most stable among Type I and Type II conformers is displayed for each family, except when the energy difference exceeds 0.2 kcal.mol^{-1}. The most stable c-DL conformer is higher in energy by 0.53 kcal.mol^{-1} than the most stable c-LL conformer.

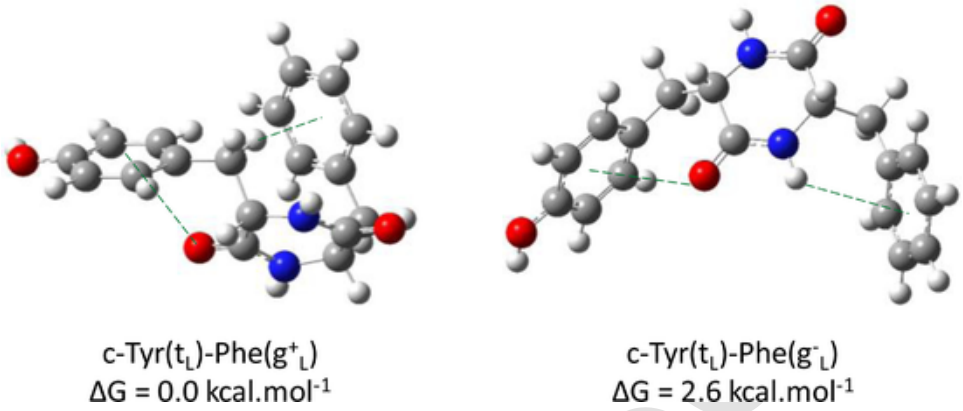

Fig. 4. Most stable calculated structures (ΔG < 3.0 kcal.mol^{-1}) of the c-LL cation. The stabilizing interactions, like the NH•••π and the interaction between the charged aromatic ring and a lone pair of the amide oxygen, are denoted by a dotted line.

family for the cation, whereas c-Tyr(t_L)-Phe(g^-_L) where both rings are extended is 2.6 kcal.mol^{-1} higher in energy. It should be noted that the neutral counterpart of the most stable form in the cation, c-Tyr(t_L)-Phe(g^+_L), is 3,8 kcal.mol^{-1} higher than the most stable neutral conformer. Conversely, the most stable neutral structure is destabilized by more than 3 kcal.mol^{-1} in the ion. NBO analysis was performed on c-Tyr(t_{LII})-Phe(g^+_L) to locate the positive charge. Most of the charge (0.785) is located on the tyrosine residue, while the phenylalanine residue only carries a charge of 0.068 and the DKP ring carries a charge of 0.146.

This analysis is in agreement with the ionization energies of p-cresol (8,17 eV) [53] and toluene (8.83 eV) [54]. Furthermore, the most stable structures found for the ion are different from those of the neutral form, as no structure with extended phenylalanine is stable for the ion. These observations are correlated to the charge localization in the ion. Indeed, as the tyrosine ring carries most of the positive charge, the NH••• π(Tyr) interaction becomes destabilizing in the cation, which disadvantages the g^- orientation of the tyrosine residue. In contrast, an interaction between the C═O and the positively charge aromatic ring of Tyr-is possible when the tyrosine is in trans orientation. Moreover, the C_βH•••π(Phe) interaction is still favorable, as the phenylalanine ring is almost neutral. This is reminiscent of what was observed in cycloPhe-Phe-and cycloTyr-Tyr-where most of the charge was borne by the extended moiety.

The calculated structures of the c-DL cation are presented in Fig. 5 and the energetics in Table S5 of the Supporting Information. NBO analysis on c-Tyr(t_{IID})-Phe(g^+_L) shows that most of the charge (0.774) is located on the tyrosine ring, while the DKP ring carries a charge of 0.161 and the phenylalanine ring carries a charge of 0.066. The most stable family is, for this diastereomer also, c-Tyr(t_D)-Phe(g^+_L), which is stabilized by the interaction between C═O and the positively charge aromatic ring of Tyr-and a C_αH•••π(Phe) interactions. The second family, c-Tyr(t_D)-Phe(g^-_L), displays the same C═O••• positive charge interaction and a NH•••π(Phe) at the expense of the C_αH•••π(Phe) interaction.

3.1.2. Electronic spectroscopy

The UV spectra of c-LL and c-DL were recorded in the region of the first electronic transition (Fig. 6). Due to the 2000 cm^{-1} energy gap between the $S_1 \leftarrow S_0$ transitions of tyrosine and phenylalanine, the first electronic transition corresponds to the excitation of tyrosine [55–59]. Both spectra present narrow lines superimposed with two broad absorption bands resulting from insufficient cooling. The origin transitions are located at 35,575 cm^{-1} for c-LL and 35,510 cm^{-1} for c-DL. For c-LL, the origin transition (A_1) is followed by a vibrational progression built on a 32 ± 2 cm^{-1} mode. Another narrow line appears at 35,591 cm^{-1} (A_2) and is followed by a progression built on a 31 ± 4 cm^{-1} mode. Two extra origin-like transitions appear at much higher wavenumbers: 35,756 cm^{-1} (B_1) and 35,817 cm^{-1} (B_2). B_1 is followed by a progression built on a 19 ± 3 cm^{-1} mode, which shows a negative anharmonicity, typical of a torsion mode. B_2 is also part of a vibrational progression built on an 18 ± 3 cm^{-1} mode. The intensity profile of the B_1 progression, with sharp decrease in intensity around 35,817 cm^{-1}, suggests the onset of a non-radiative process. Some extra lines are not part of any vibrational progression and appear at 25, 31, 42, 183 and 274 cm^{-1} above A_1.

The c-DL spectrum is similar to that of c-LL. Indeed, four origin-like transitions followed by progressions are observed, separated into two

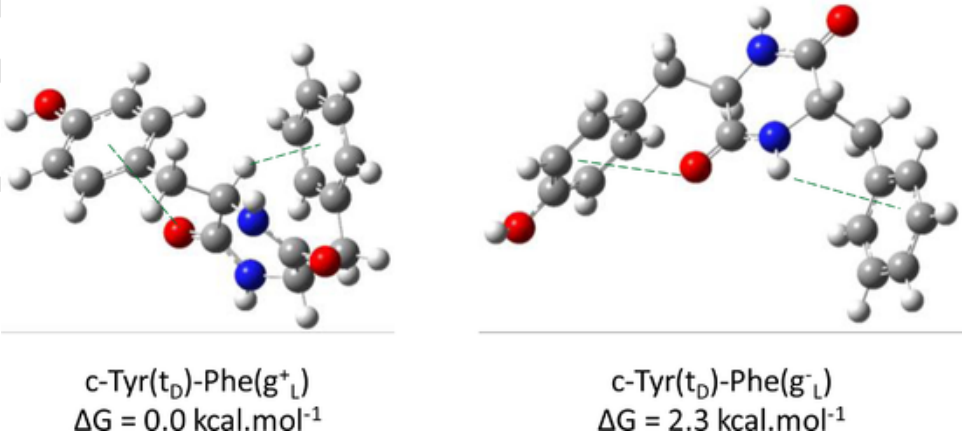

Fig. 5. Most stable calculated structures (ΔG < 3.0 kcal.mol^{-1}) of the c-DL cation. The stabilizing interactions are denoted by a dotted line, as in Fig. 4.

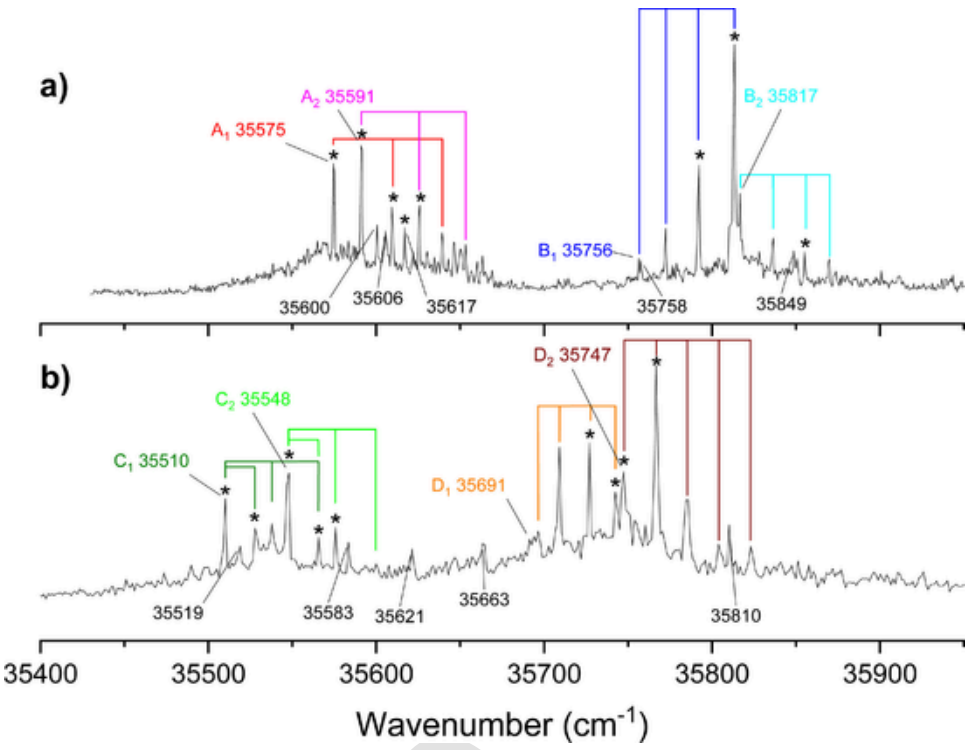

Fig. 6. One-color resonant two-photon ionization spectra of the S_0-S_1 transition of the cycloTyr-Phe-diastereomers: a) c-LL and b) c-DL. The asterisks * mark the band position where the IR-UV double resonance spectra were recorded. The comb-shaped patterns materialize the bands belonging to a vibrational progression (see text), indicated by A_1, A_2, B_1, B_2 for c-LL and C_1, C_2, D_1, D_2 for c-DL.

groups: C_1 at 35,510 cm^{-1} followed by a progression built on a 28 cm^{-1} mode, C_2 at 35,548 cm^{-1} followed by a progression built on a 26 ± 2 cm^{-1} mode, D_1 at 35,691 cm^{-1} followed by a progression built on a 17 ± 1 cm^{-1} mode and D_2 at 35,747 cm^{-1} followed by a progression built on a 19 ± 1 cm^{-1} mode. Some extra bands appear at 9, 18, 73, 111, 153 and 300 cm^{-1} above C_1. The +18 band may result from a 18 cm^{-1} mode for C_1, which may be also present for C_2, if we assume that two lines are superimposed, namely C_2 + 18 and C_1 + 56.

All these features suggest the coexistence of four conformers for each diastereomer. The lower energy transitions for c-LL and for c-DL are in the same range as the origin transitions of the tyrosine conformers (35,491 cm^{-1} – 35,650 cm^{-1}) [36, 38]. In contrast, the origin-like transitions B_1, B_2, D_1 and D_2 are higher in energy, which suggests that the tyrosine chromophore is in a different environment in the two conformers. The UV spectrum of c-DL was also recorded near the region of the $S_1 \leftarrow S_0$ transition of the phenylalanine chromophore (37,537 cm^{-1} – 37,613 cm^{-1} depending on the conformers) [55, 59] (see Fig. S2 of the SI). It displays a narrow line at 37,373 cm^{-1}, superimposed with a background, which must correspond to a $S_2 \leftarrow S_0$ vibronic transition of one of the conformers.

3.1.3. *Vibrational spectroscopy of the neutral molecules and assignment*

In order to shed light on the structure of the conformers detected, the double resonance spectra of c-LL and c-DL were recorded setting the UV probe on the transitions marked with an asterisk * in Fig. 6. The spectra obtained by setting the UV probe at 35,591 cm^{-1} (A_2 band) and 35,813 cm^{-1} (most intense band of the B_1 progression) for c-LL and at 35,548 cm^{-1} (C_2 band) and 35,766 cm^{-1} (most intense band of the D_2 progression) for c-DL are shown in Fig. 7. For c-LL, the infrared spectra were identical whether setting the probe on transitions from the A_1, A_2 (A group), B_1 and B_2 (B group) progressions. A congested triplet appears between 3399 cm^{-1} and 3424 cm^{-1}, in the ν(NH) stretch range. An absorption band is observed at 3655 ± 1 cm^{-1}, which is typical of a free phenol ν(OH) [3, 5, 35-38]. However, two different vibrational spectra were obtained for the C_1 and C_2 progressions (C group) and the D_1 and D_2 progressions (D group) of c-DL. The difference lies in the ν(OH) stretch region; the absorption band in the C group appears at 3656 cm^{-1} vs. 3653 cm^{-1} in the D group. In addition, the ν(NH) stretch region differs from c-LL, with a large gap between the lower-energy band (3393 cm^{-1}) and a doublet at 3422 /3432 cm^{-1}.

The simulated spectra of the most stable calculated structures are compared to the experiment in Fig. 7. For c-LL, the simulated spectra are the same regardless of the family and of the orientation of the phenol OH (Type I/ Type II conformers). The ν(NH) stretch frequency around 3400 cm^{-1} is well reproduced, with only a 4 cm^{-1} error. For c-Tyr(g^-_{LI})-Phe(g^+_L) and c-Tyr(g^-_{LII})-Phe(g^+_L), this band is assigned to the NH bond in interaction with the tyrosine ring, whereas in c-Tyr(g^+_{LI})-Phe(g^-_L) and c-Tyr(g^+_{LII})-Phe(g^-_L), it is assigned to the NH bond in interaction with the phenylalanine ring. Therefore, the strength of the NH•••π interaction does not seem to depend on the nature of the aromatic ring. For all conformers, the ν(NH) transition around 3422 cm^{-1} is assigned to the free NH (3405 cm^{-1} in the simulations). However, the band at 3412 cm^{-1} in the ν(NH) region is not predicted in the harmonic approximation and may be a combination band or an overtone. To confirm this hypothesis, a full anharmonic frequency calculation was performed for the most stable conformer of c-LL. The simulated spectrum is shown in Fig. S3 of the SI. It displays overtone bands due to two quanta of the antisymmetric ν(C═O) stretch and combination bands involving both the asymmetric and symmetric ν(C═O) stretching modes, as suggested in cycloTyr-Tyr-and cycloPhe-Phe [3, 5, 32]. The predicted OH stretch frequency is the same for all the conformers, and compares well with the experimental value, which confirms the lack of OH•••π interaction. Unfortunately, the IR spectra do not help for the conformational assignment.

The simulated spectra of c-DL are quite similar to those of c-LL and leads to the same assignment. The main difference is the larger gap between the ν(NH) stretch frequencies calculated in c-DL, also seen in the experimental spectra. The simulated spectra of the c-DL conformers are slightly different from each other. Indeed, the first stretch frequency assigned to the NH bond in interaction with an aromatic ring is predicted

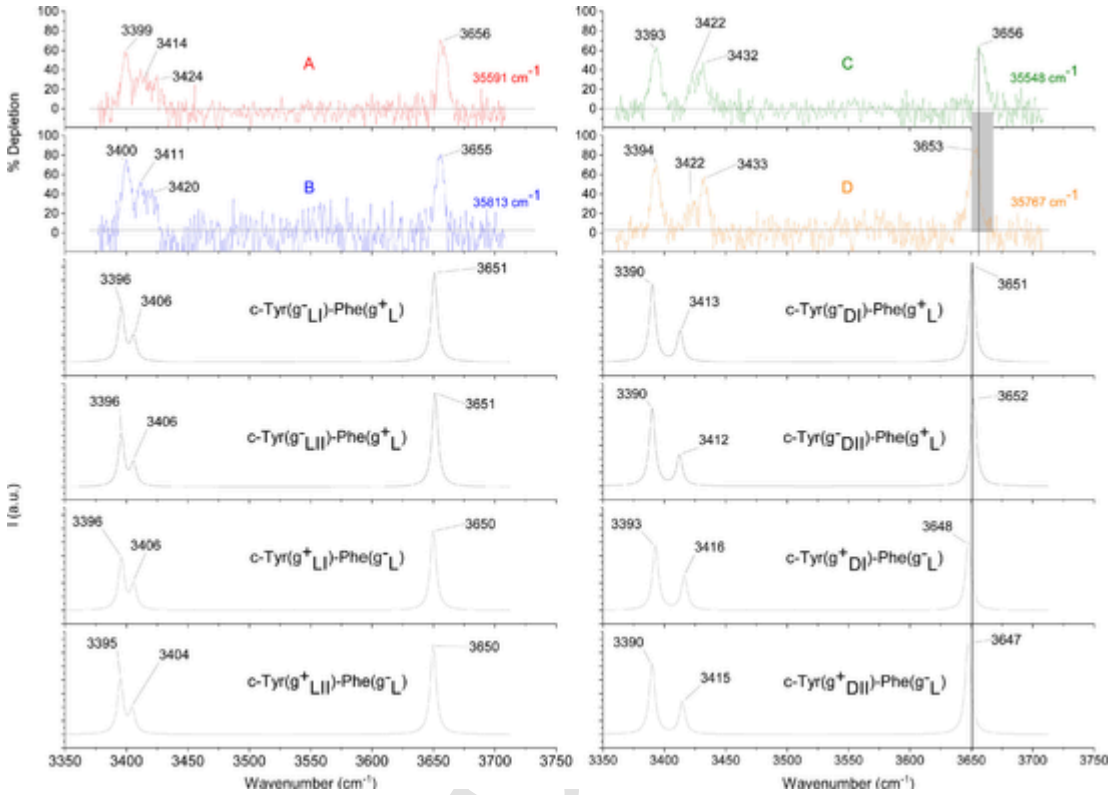

Fig. 7. Comparison between the IR/UV double resonance spectra of c-LL (left) and c-DL (right) and those simulated for the most stable structures. The A, B, C and D spectra are obtained by probing one of the vibrational bands of the A, B, C, D vibrational progressions observed in the S_0-S_1 spectra shown in Fig. 6.The probe UV wavelength was fixed at 35,591, 35,813, 35,548 and 35,767 cm^{-1}, respectively.

at 3390 cm^{-1} for c-Tyr(g^-_{DI})-Phe(g^+_L), c-Tyr(g^-_{DII})-Phe(g^+_L) and c-Tyr(g^+_{DII})-Phe(g^-_L), but is predicted at 3393 cm^{-1} for c-Tyr(g^+_{DI})-Phe(g^-_L). According to Table S3 in the SI, the distance between NH and the chromophore in c-Tyr(g^+_{DI})-Phe(g^-_L) is 0.10 Å larger than in the other conformers, which could explain the higher stretch frequency. Unfortunately, this difference was not observed experimentally: the vibration appears at 3393 cm^{-1} or 3394 cm^{-1} for each electronic transition probed. Moreover, the band assigned to the free NH (calculated around 3414 cm^{-1}) is slightly different for each conformer in the simulated spectra, but this difference is not seen in the experiment; all the spectra showing a value of 3432 cm^{-1}. This is probably due to the deficiency of the harmonic approximation. The experimental transition at 3422 cm^{-1}in the ν(NH) stretch region is assigned to the ν(C═O) overtone. The frequency of the free ν(NH) is underestimated by 17 to 20 cm^{-1} in the simulations. It is important to note that the ν(OH) stretch frequency is predicted to be blue shifted by 4 cm^{-1} for c-Tyr(g^+_D)-Phe(g^-_L) compared to c-Tyr(g^-_D)-Phe(g^+_L), and this shift is observed experimentally. Thus, this slight difference allows assigning bands from the C group to c-Tyr(g^-_D)-Phe(g^+_L) and bands from the D group to c-Tyr(g^+_D)-Phe(g^-_L). Unfortunately, we cannot go further and assign one progression to a given conformer, because the infrared technique is not sensitive to the position of the hydroxyl on the tyrosine chromophore [3, 5, 35-38]. This assignment is confirmed by the comparison with cycloTyr-Tyr, for which the $S_1 \leftarrow S_0$ transition was localized on the extended tyrosine ring, whereas the $S_2 \leftarrow S_0$ transition was localized on the folded tyrosine ring [5]. Here, as the electronic spectra are recorded in the $S_1 \leftarrow S_0$ transition region of the tyrosine ring, the lower transition is expected to belong to the structure with the tyrosine ring extended. Therefore bands from the C group would belong to c-Tyr(g^-_D)-Phe(g^+_L) and bands from the D group to c-Tyr(g^+_D)-Phe(g^-_L). A and B progressions can be assigned on the same basis: the A_1 and A_2 progressions correspond to the family where the tyrosine ring is extended, c-Tyr(g^-_L)-Phe(g^+_L), and the B_1 and B_2 progressions to the family with extended phenylalanine ring, c-Tyr(g^+_L)-Phe(g^-_L).

3.1.4. Vibrational spectroscopy of the ions and comparison with the simulations

The IR spectra of the cations were recorded by monitoring the depletion of the signal at the mass of the parent at m/z = 310 (Fig. 8) and the increase of the m/z = 204 fragment signal (Fig. S4 of the SI), which corresponds to the loss of *p*-quinomethide (106 amu) from the tyrosyl ring. This fragmentation results from a C_α-C_β cleavage concomitant with an hydrogen atom migration, already observed in the collision-induced dissociation of radical cations of tyrosine-containing peptides, [60] in the mass spectrum resulting from photoionization of cycloTyr-Tyr-or cycloTyr-Pro-and in the electron impact ionization of tyrosine-containing DKP peptides [3, 5, 61].

For each diastereomer, the IR spectrum is the same regardless of the probed electronic transition.

The two experimental spectra slightly differ from each other in the ν(NH) region: the ν(NH) stretch is 7 cm^{-1} higher in frequency in c-DL than in c-LL, but these values are close to that observed in neutral cyclo-Tyr-Phe. In contrast, the ν(OH) stretch frequency, identical for both diastereomers, is very different from that in the neutral molecules. It appears around 3570 cm^{-1} instead of 3655 cm^{-1}, which is the consequence of the important positive partial charge localized on the tyrosine cycle. This value is the same as in the cycloTyr-Tyr-cation [5] but is shifted up compared to the cycloTyr-Pro-cation (3565 cm^{-1}) [3] and to the phenol cation (3534 cm^{-1}) [62].

The simulated spectra of the most stable structures are compared to the experiment in Fig. 8. They are the same regardless of the orientation of the hydroxyl group. The simulated spectrum of c-Tyr(t_L)-Phe(g^+_L) shows two transitions close in energy around 3400 cm^{-1}, which could not be resolved in the experiment. This may be due to an insufficient signal to noise ratio. This may also result from the fact that the ion is vi-

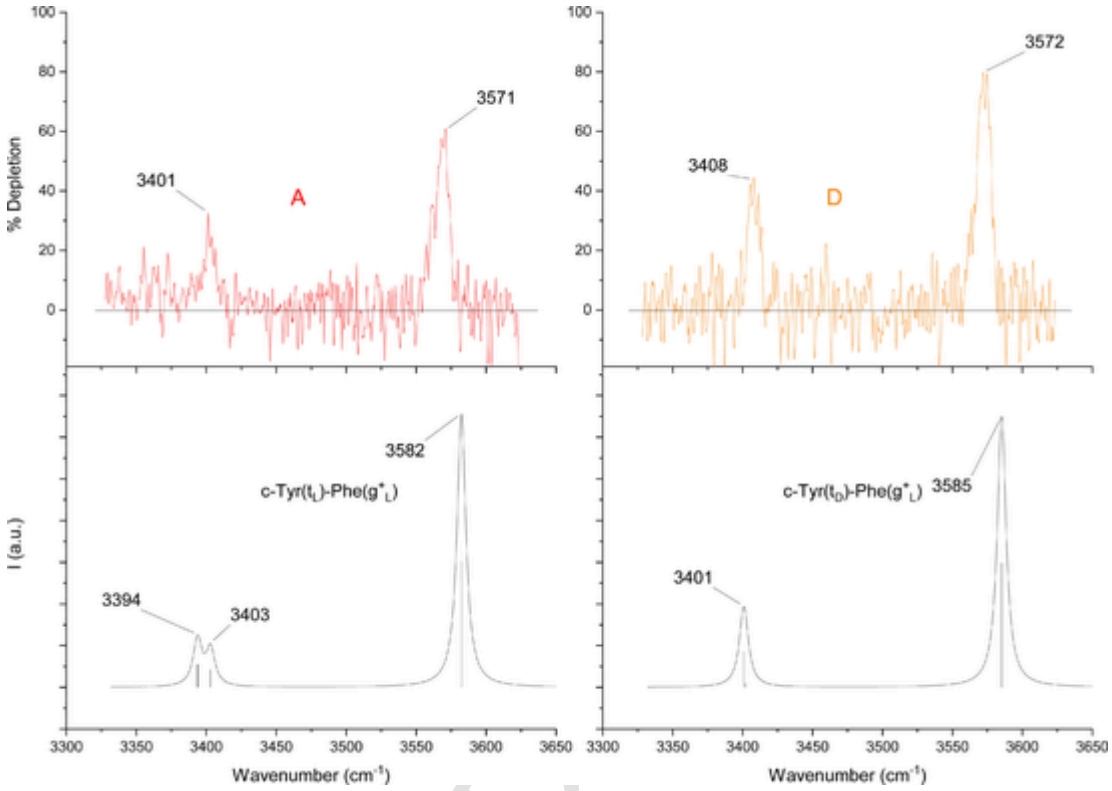

Fig. 8. Comparison between the UV/IR double resonance spectra of the c-LL (left) and c-DL (right) cations and those simulated for the most stable structures. The probe UV wavelength was fixed at 35,591(A) and 35,767 cm^{-1} (C) for c-LL^+ and c-DL^+, respectively. The spectra of c-LL^+ (c-DL^+) are identical to A (D) when probing the bands at 35,813 (35,548 cm^{-1}), respectively.

brationally hot due to the excess energy in the cation resulting from the two-photon ionization (of ~5600 cm^{-1} by taking the adiabatic ionization energy of p-cresol) [53]. This can also explain the overestimation by 12 cm^{-1} of the simulations for the ν(OH) stretch frequency.

3.2. Solid state structure

3.2.1. Crystallographic structure

The crystal structure of c-LL is shown in Fig. 9 and the main structural parameters are listed in Table 1. c-LL crystallizes in the Sohncke orthorhombic space group $P2_12_12_1$ containing three two-fold screw axes. The asymmetric unit is composed of one molecule, and the unit cell of the crystal is displayed in Fig. S5 of the SI. The crystal is composed of infinite strands of identical conformers parallel to the a axis and bound by two intermolecular NH•••O═C hydrogen bonds in a β-sheet like fashion, as seen in Fig. 9(c). This β-sheet pattern is also often observed in gas-phase peptide dimers, including the cycloLPhe-LPhe dimer [6, 63]. The monomers adopt the c-Tyr(g^+_{LI})-Phe(g^-_L) conformation, which was found to be the most stable along with c-Tyr(g^+_{LII})-Phe(g^-_L) in the gas phase. This is quite similar to the cycloLPhe-LPhe crystal, [64] which crystallizes in the $P22_12_1$ space group, in which one of the screw axes of $P2_12_12_1$ is replaced by a C2 rotation around the a axis. The cycloLPhe-LPhe crystal also contains the most stable conformation of the monomers with one phenylalanine ring folded and the other one extended, bound by double NH•••O═C bonds [64]. In both systems, the extended aromatic rings, *i.e.* the benzene ring in cycloTyr-Phe, are in a stacked geometry while the folded aromatic rings, *i.e.* the phenol rings in cycloTyr-Phe, are in a parallel displaced arrangement.

Cyclo LTyr-LPhe differs from cycloLPhe-LPhe by the fact that the tyrosine phenol group enables an additional interaction. Each strand is then bound to two adjacent ones by OH•••O═C hydrogen bonds (Fig. 9, (b and c)), with the tyrosine amide C═O interacting with both NH and OH groups in a bifurcated manner. Within a strand, each monomer is strongly bound to its two neighbors thanks to strong hydrogen bonds, but the additional hydrogen bonds between the strands are quite weak, as manifested by the long OH•••O distance and the $\widehat{O_2H_3O_3}$ angle of 122°, far from the 180° optimal value. The additional OH•••O interaction results in conformation locking of cycloTyr-Phe-in the solid state. The phenol hydroxyl must be in I position and the tyrosine must be folded to make the formation of a H-bond possible. Hence the c-Tyr(g^-_L)-Phe(g^+_L) family, which is only 0.4 kcal.mol^{-1} higher in energy in the gas phase, is not present in the crystal. Comparison between the cycloLPhe-LPhe [64] and cycloLTyr-LPhe crystals leads to the conclusion that the dissymmetry brought upon by the presence of two different rings has smaller consequences on the dissymmetry of the NH•••O hydrogen bonds than that related to the folded/extended nature of the aromatic rings (see Table 1).

3.2.2. Infrared spectra

The experimental infrared absorption spectrum of c-LL in the solid phase is shown in Fig. 10(A). It displays two intense bands in the amide I (C═O stretch) region, at 1657 cm^{-1} and 1678 cm^{-1}, accompanied by two weak side bands, at 1589 and 1616 cm^{-1}, and a stronger band at 1518 cm^{-1}. The amide II region (β(NH)) is composed of a broad feature at 1466 cm^{-1}. This spectrum is very similar to that of cycloLPhe-LPhe, except for the 1657 cm^{-1} band which is shifted down in frequency by 6 cm^{-1} in cycloLTyr-LPhe [15]. The experimental spectrum is compared to that simulated for the monomer present in the crystal, c-Tyr(g^+_{LI})-Phe(g^-_L), in Fig. 10(B). It shows two superimposed ν(C═O) bands, thus at odd with the experiment that shows a doublet in this range. This doublets suggests that the C═O groups are not in the same environments, as for cycloLPhe-LPhe, where dimers accounted for the experimental results. [15] Therefore, the dimer bound by two NH•••C═O hydrogen bonds extracted from the crystal structure (Fig. 9, (a)) was optimized. Its IR absorption spectrum is displayed in Fig. 10 (C). The calculated infrared spectrum satisfactorily reproduces the dou-

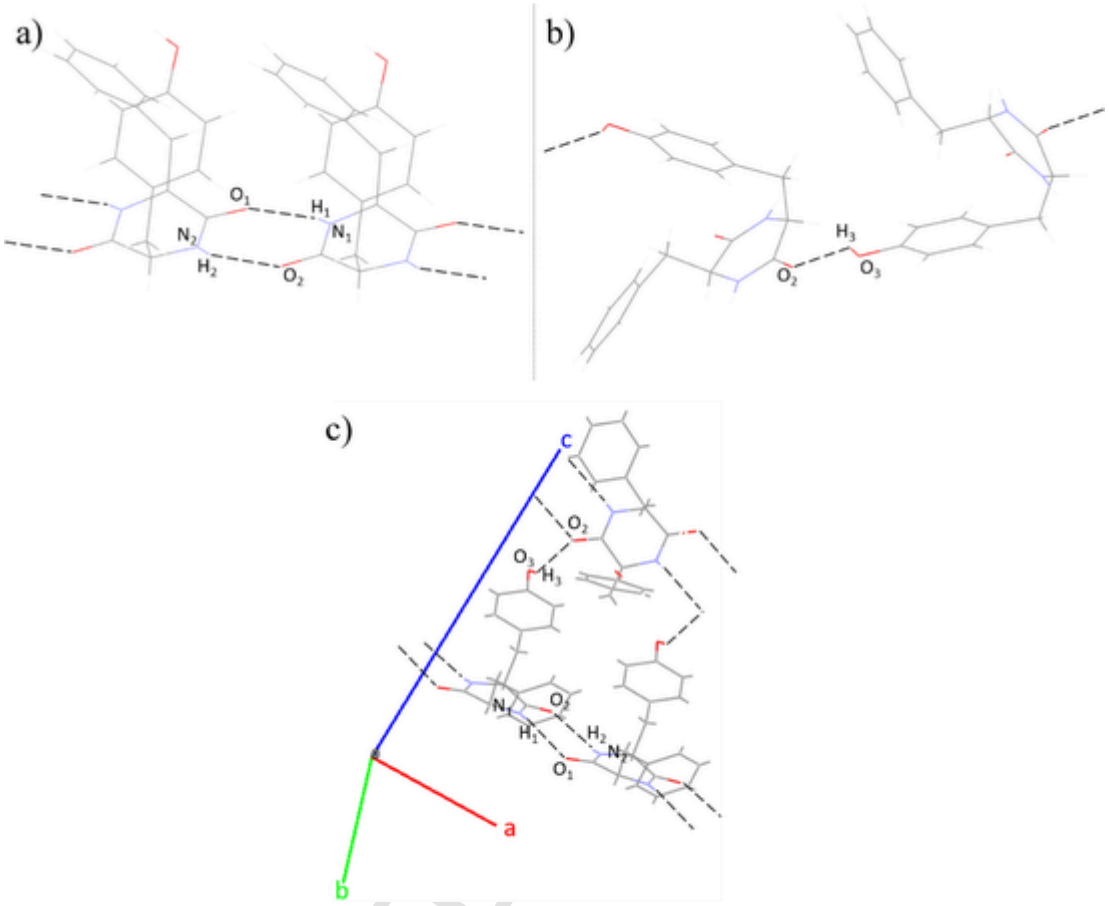

Fig. 9. Crystallographic structure of c-LL: (a) dimer extracted from the infinite strands bound by NH•••O═C hydrogen bonds, (b) infinite strands bound by OH•••O═C hydrogen bonds, (c) a, b and c axis of the crystal.

Table 1
Structural parameters of the hydrogen bonds in the crystallographic structure. The data for cycloPhe-Phe-are also given for the sake of comparison. In cycloPhe-Phe, the index "1" and "2" denote the amide of the extended and folded residue, respectively.

	(O•••H) distance (Å)	(OH•••N) angle (°)
Cyclo LTyr-LPhe		
C═O_1•••H_1—N_1	2.04	165.6
C═O_2•••H_2—N_2	2.08	153.6
C═O_2•••H_3—O_3	2.61	122.0
Cyclo LPhe-LPhe		
C═O_1•••H_1—N_1	2.01	140.9
C═O_2•••H_2—N_2	1.87	157.9

blet in the amide I region: the higher frequency band corresponds to the two free ν(C═O) stretches coupled to the adjacent free β(NH) bends and the lower frequency band corresponds to the antisymmetric bound ν(C═O) stretch coupled to the antisymmetric β(NH) bend. The gap between the free ν(C═O) and the bound ν(C═O) is 28 cm^{-1}, larger than the experimental value by 7 cm^{-1}. The 6 cm^{-1} difference between cycloLTyr-LPhe and cycloLPhe-LPhe observed for the lower frequency ν(C═O) stretch may suggest different bonding patterns, thus reflecting the presence of the OH of the tyrosine ring. This is why the tetramer extracted from the crystal structure, namely two β-sheet type dimers bound by two C═O•••HO hydrogen bonds, was also optimized. Its structure is shown in Fig. 10(F) and the corresponding IR absorption in Fig. 10(D). The gap between the free ν(C═O) and the bound ν(C═O) stretches is 41 cm^{-1}, which is much higher than the experimental value. This shows that the β-sheet arrangement dictates the geometry of the C═O•••HO hydrogen bond, and that considering the tetramer leads to an overestimation of the influence of the C═O•••HO interaction. The monomer and this tetramer are then ruled out, based on the amide I region. A larger β-sheet aggregate is also ruled out given the intensities ratio for the free and bound ν(C═O) stretches, suggesting the presence of dimers in the powder, as seen in cycloLPhe-LPhe [15].

3.2.3. *VCD spectra*

The experimental VCD and IR absorption spectra of c-LL are shown in Fig. 11(A). The raw VCD spectra of c-LL and c-DD are shown in Fig. S6 of the SI. The experimental VCD spectrum is dominated by an intense bisignate signature in the ν(C═O) region. The weak bands at 1590 and 1616 cm^{-1} both show a positive VCD signal. As observed for the IR absorption, the VCD spectra of the monomer and the tetramer do not account for the experimental results (see Fig. S7 of the SI). The experimental spectrum is compared to the calculated spectrum of the dimer extracted from the crystal structure in Fig. 11(B). The bound ν(C═O) region shows a weak exciton coupling [65] not seen in the experiment; the antisymmetric ν(C═O) stretch shows a weak negative signal, whereas the symmetric ν(C═O) stretch shows a strong positive signal. During the optimization, the geometry of the dimer changes, in particular the aromatic rings become less parallels to each other. It is possible that this dimer does not reflect the structure of the powder. This is why other conformations of β-sheet type dimers have been optimized, with different orientations of the cycles. The IR spectra for all the dimers are consistent with the experiment (Fig. S8). The most stable one (Fig. 11(C)) is composed of the most stable conformation of the monomer c-Tyr(g^+_{LII})-Phe(g^-_L) and of the stacked conformation c-Tyr(g^+_{LI})-Phe(g^+_L). The two tyrosyl groups are bound by an OH•••OH hydrogen bond, which stabilizes the structure. Its infrared spectrum is

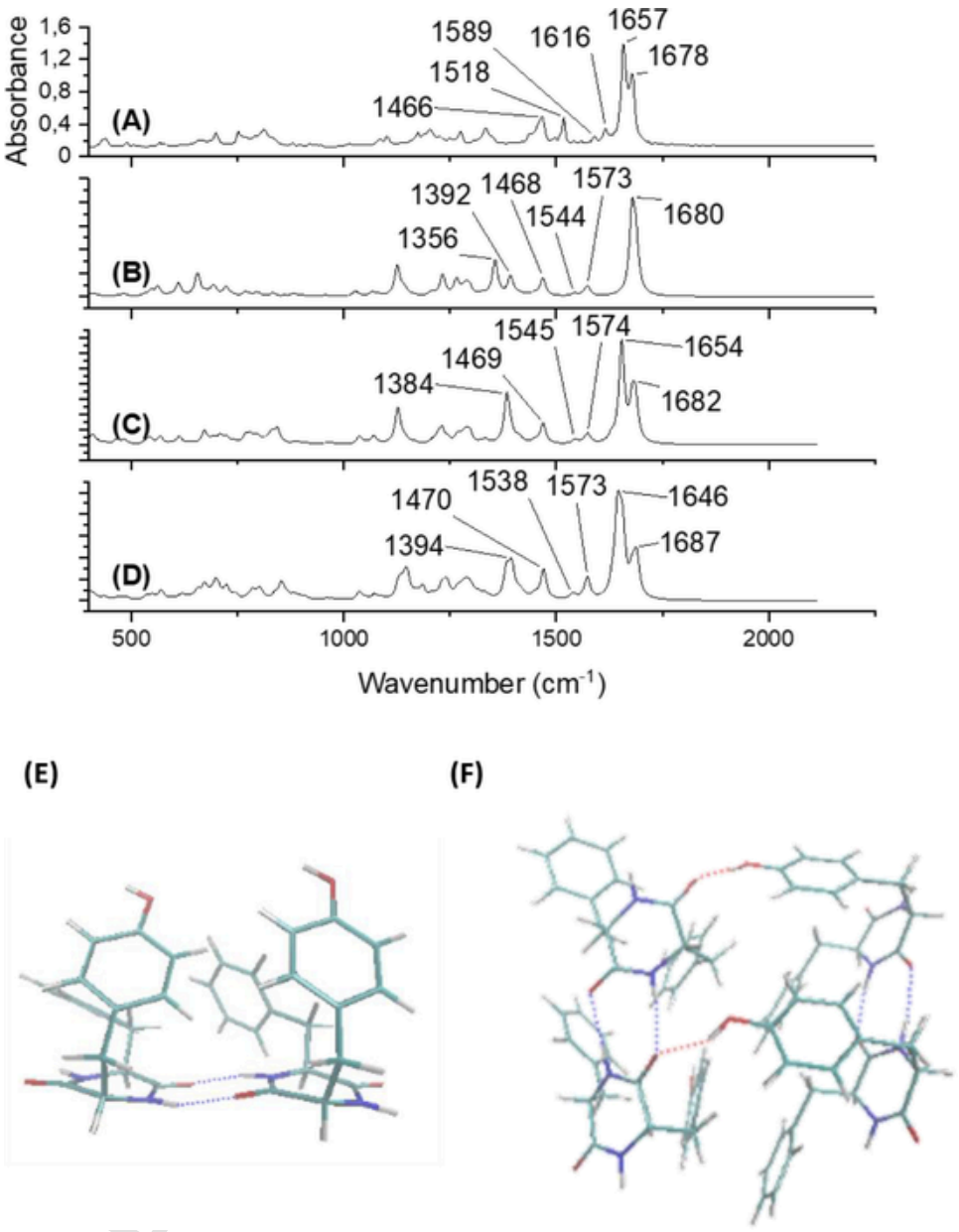

Fig. 10. (A) Experimental infrared absorption spectrum of c-LL in KBr; (B) Calculated infrared absorption spectrum of the monomer c-Tyr(g^{+}_{LL})-Phe(g^{-}_{L}); (C) Calculated infrared absorption spectrum of the dimer extracted from the crystal structure; (D) Calculated infrared spectrum of the tetramer extracted from the crystal structure; (E) Structure of the dimer extracted from the crystal structure after optimization; (F) Structure of the tetramer extracted from the crystal structure after optimization.

very similar to that of the dimer extracted from the crystal. It reproduces well the experimental bisignate signature in the ν(C═O) stretch region, which does not result from exciton coupling, but from two VCD bands opposite in sign corresponding to the bound and the free C═O stretches, as observed for cycloPhe-Phe [15]. However, the simulated aromatic ν(C═C) region around 1600 cm^{-1} is characterized by an exciton splitting, which is not observed in the experiment. Besides, the VCD bands corresponding to the aromatic β(CH) and β(NH) at 1518 and 1466 cm^{-1}, respectively, are too strong compared to the experiment. Other dimers were then optimized. Inclusion of dispersion corrections did not improve the agreement between simulated and experimental spectra, as already observed in VCD spectroscopy, [66–68] nor did optimization of structures in which the position of the aromatic ring is kept frozen in the geometry of the crystal. The best match with the experiment is shown in Fig. 11(D). This dimer is composed of two monomers with the folded-folded conformation, one stacked and the other one in a T-shaped conformation, bound by an OH•••OH hydrogen bond. It should be noticed that this dimer therefore reproduces the different interactions at play in the crystal, namely, the two NH•••OC and the OH•••O hydrogen bonds. Its simulated infrared spectrum is identical to that of the other calculated dimers and it reproduces well the bisignate signature in the ν(C═O) region. The region of the aromatic β(CH) and β(NH) bends is better reproduced in terms in intensity. However, the aromatic ν(C═C) stretch region still shows an exciton splitting. Its VCD might be really sensitive to the rotations of the aromatic rings. The stacked or T-shaped conformations are then likely to be present in the powder, which shows a rearrangement from the crystal structure or the gas phase, where only the folded-extended conformations are seen. More details about the optimized structures of the dimers can be found in Table S6 of the SI. The theoretical $\Delta\varepsilon/\varepsilon$ values for the ν(C═O) stretches are underestimated by the calculations by one order of magnitude. This may arise from non-local effects in the crystal packing which

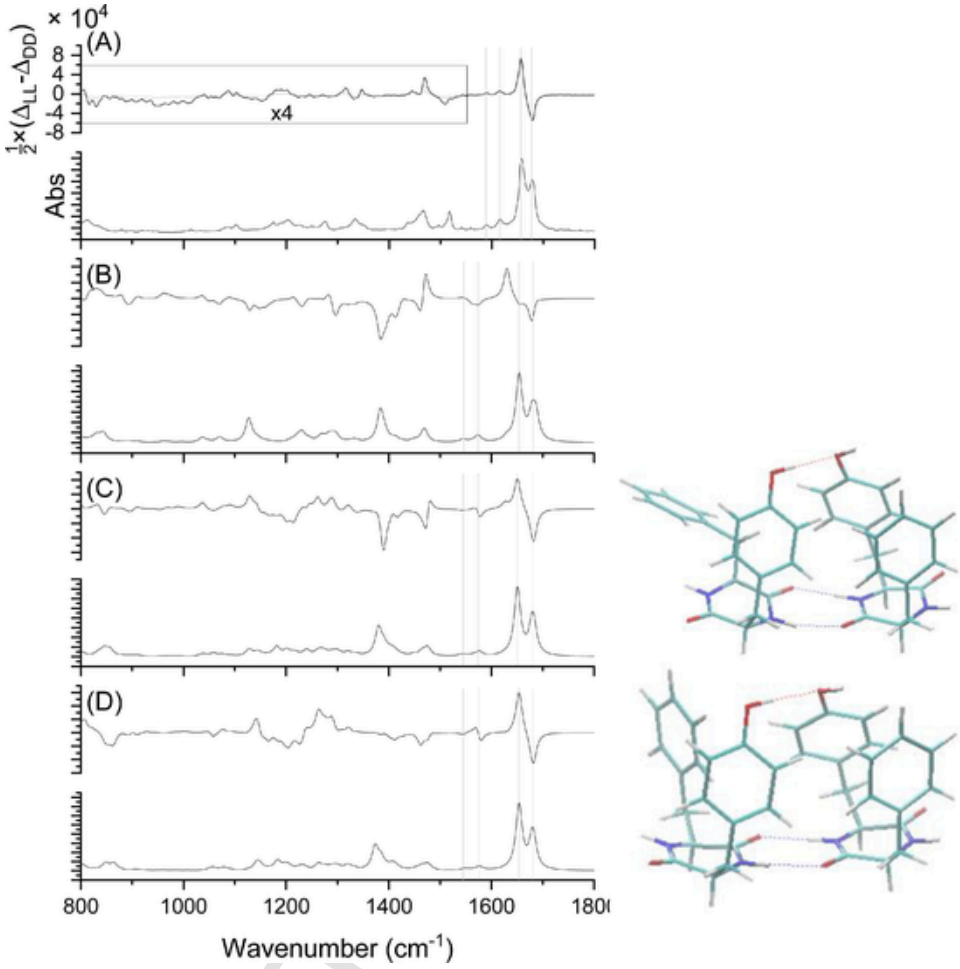

Fig. 11. (A) Experimental VCD and IR absorption spectra of c-LL (half difference of the VCD spectra of c-LL and c-DD); (B) Calculated VCD and IR absorption spectra of the dimer extracted from the crystal structure; (C) Calculated VCD and IR spectra of the most stable dimer and its structure; (D) Calculated VCD and IR spectra of the dimer with the best VCD spectrum and its structure.

enhance the VCD signal, as already shown for the ν(C═O) stretches in L-alanine [41].

4. Conclusion

Each cycloTyr-Phe-diastereomer shows two families of conformers under supersonic expansion conditions. In one of them, the tyrosine ring is folded over the DKP ring and the phenylalanine ring extended outwards, and *vice versa* in the other one. Both conformers are stabilized by weak NH•••π and CH•••π interactions. Because of the rigidity of the DKP ring, a stacked conformation of c-LL involving an OH•••π interaction is not stable in the gas phase, which contrasts with the conclusions drawn from NMR experiments in a DMSO solution [8]. For c-LL, the vibrational spectra of the two families of conformers are identical and do not provide a clear assignment of the peaks observed in the REMPI spectrum. In contrast for c-DL, the ν(OH) frequency is slightly different for the two families and enables the assignment of the conformation with the lower $S_1 \leftarrow S_0$ transition to the structure with the extended tyrosine ring. This assignment is consistent with the localization of the $S_1 \leftarrow S_0$ and $S_2 \leftarrow S_0$ transitions previously calculated for cyclo-Tyr-Tyr [5]. The differences between the two diastereomers are minor, as seen in cycloPhe-Phe [4]. The CH•••π interaction involves the C_β in c-LL whereas it involves the C_α in c-DL, and the NH•••π interaction is stronger in c-DL than in c-LL. The ion shows the Tyr-in an extended *trans* geometry dictated by the localization of the charge on the phenol ring.

The crystallographic structure of c-LL contains the monomers in their most stable conformation bound by strong NH•••O═C interactions and weak OH•••O═C interactions. Comparison between the experiment and the simulated infrared spectra suggests that dimers are likely to be present in the powder. The structure of the dimers is however different in the crystal and in the powder. Dimers composed of monomers in a folded-folded conformation (stacked or T-shaped) reproduce the experimental VCD spectrum better. This shows a rearrangement in a powder compared to the crystal and the gas phase. The intensities of the VCD signals of the ν(C═O) stretches are underestimated by the calculations. This can be explained by the non-local effects in the crystal packing, which enhance the VCD signal [40, 41].

5. Author contribution

Jennifer Dupont: Experimental investigation, Data curation, Quantum chemistry calculations, Writing- Original draft preparation, Reviewing and Editing Régis Guillot crystallographic measurements Writing- Original draft preparation Valeria Lepere: Experimental Investigation, Writing- Reviewing and Editing. Anne Zehnacker: Conceptualization, Quantum chemistry calculations, Experimental investigation, Writing- Reviewing and Editing.

6. Crystallographic data

Crystal data have been deposited at the Cambridge Crystallographic Database with CCDC number 2143350 which contain the supplemen-

tary crystallographic data for this paper. These data can be obtained free of charge from The Cambridge Crystallographic Data centre via www.ccdc.cam.ac.uk/data_request/cif.

Declaration of Competing Interest

The authors declare that they have no known competing financial interests or personal relationships that could have appeared to influence the work reported in this paper.

Acknowledgment

This work has been supported by the French National Research Agency (ANR) Dichroprobe project (Grant ANR-18-CE29-0001-01). We acknowledge the computing center MésoLUM managed by ISMO (UMR8214) and LPGP (UMR8578), University Paris-Saclay (France). We thank Yassin El Koulali for experimental assistance.

Supplementary materials

Supplementary material associated with this article can be found, in the online version, at doi:10.1016/j.molstruc.2022.133059.

References

[1] A.D. Borthwick, 2,5-diketopiperazines: synthesis, reactions, medicinal chemistry, and bioactive natural products, Chem. Rev. 112 (7) (2012) 3641–3716.
[2] S.N. Kumar, C. Dileep, C. Mohandas, B. Nambisan, C.A. Jayaprakas, Cyclo(D-Tyr-D-Phe): a new antibacterial, anticancer, and antioxidant cyclic dipeptide from Bacillus sp N strain associated with a rhabditid entomopathogenic nematode, J. Peptide Sci. 20 (3) (2014) 173–185.
[3] A. Pérez-Mellor, I. Alata, V. Lepère, A. Zehnacker, Conformational study of the jet-cooled diketopiperazine peptide cyclo tyrosyl-prolyl, J. Phys. Chem. B 123 (28) (2019) 6023–6033.
[4] A. Pérez-Mellor, I. Alata, V. Lepere, A. Zehnacker, Chirality effects in the structures of jet-cooled bichromophoric dipeptides, J. Mol. Spectrosc. 349 (2018) 71–84.
[5] F. BenNasr, A. Pérez-Mellor, I. Alata, V. Lepere, N.E. Jaidane, A. Zehnacker, Stereochemistry-dependent hydrogen bonds stabilise stacked conformations in jet-cooled cyclic dipeptides: (LD) *vs.* (LL) cyclo tyrosine-tyrosine, Faraday Discuss. 212 (2018) 399–419.
[6] S. Bakels, I. Stroganova, A.M. Rijs, Probing the formation of isolated cyclo-FF peptide clusters by far-infrared action spectroscopy, Phys. Chem. Chem. Phys. 23 (37) (2021) 20945–20956.
[7] E.H. Strickland, M. Wilchek, J. Horwitz, C. Billups, Low Temperature circular dichorism of tyrosyl and tryptophanyl diketopiperazines, J. Biol. Chem. 245 (16) (1970) 4168, -+.
[8] T. Yamazaki, K.I. Nunami, M. Goodman, Cyclic retro-inverso dipeptides with 2 aromatic side-chains .2. conformational-analysis, Biopolymers 31 (13) (1991) 1513–1528.
[9] G. Pohl, E. Gorrea, V. Branchadell, R.M. Ortuno, A. Perczel, G. Tarczay, Foldamers of beta-peptides: conformational preference of peptides formed by rigid building blocks. The first MI-IR spectra of a triamide nanosystem, Amino Acids 45 (4) (2013) 957–973.
[10] G. Magyarfalvi, G. Tarczay, E. Vass, Vibrational circular dichroism, Wiley Interdiscipl. Rev. Comput. Mol. Sci. 1 (3) (2011) 403–425.
[11] S. Gobi, K. Knapp, E. Vass, Z. Majer, G. Magyarfalvi, M. Hollosi, G. Tarczay, Is beta-homo-proline a pseudo-gamma-turn forming element of beta-peptides? An IR and VCD spectroscopic study on Ac-beta-HPro-NHMe in cryogenic matrices and solutions, Phys. Chem. Chem. Phys. 12 (41) (2010) 13603–13615.
[12] T.A. Keiderling, Structure of condensed phase peptides: insights from vibrational circular dichroism and raman optical activity techniques, Chem. Rev. 120 (7) (2020) 3381–3419.
[13] A. Pérez-Mellor, K.L. Barbu-Debus, A. Zehnacker, Solid-state synthesis of cyclo LD-diphenylalanine: a chiral phase built from achiral subunits, Chirality 32 (5) (2020) 693–703.
[14] V. Declerck, A. Pérez-Mellor, R. Guillot, D.J. Aitken, M. Mons, A. Zehnacker, Vibrational circular dichroism as a probe of solid-state organisation of derivatives of cyclic beta-amino acids: cis- and trans-2-aminocyclobutane-1-carboxylic acid, Chirality 31 (8) (2019) 547–560.
[15] A. Pérez-Mellor, A. Zehnacker, Vibrational circular dichroism of a 2,5-diketopiperazine (DKP) peptide: evidence for dimer formation in cyclo LL or LD diphenylalanine in the solid state, Chirality 29 (2) (2017) 89–96.
[16] D. Scuderi, K.L. Barbu-Debus, A. Zehnacker, The role of weak hydrogen bonds in chiral recognition, Phys. Chem. Chem. Phys. 13 (40) (2011) 17916–17929.
[17] E.T. Mengesha, A. Zehnacker-Rentien, J. Sepiol, M. Kijak, J. Waluk, Spectroscopic study of jet-cooled deuterated porphycenes: unusual isotopic effects on proton tunneling, J. Phys. Chem. B 119 (6) (2015) 2193–2203.
[18] R.N. Pribble, T.S. Zwier, Size-specific infrared-spectra of benzene-$(H_2O)_{(n)}$ clusters (n = 1 through 7) - evidence for noncyclic $(H_2O)_{(n)}$ structures, Science 265 (5168) (1994) 75–79.
[19] S. Tanabe, T. Ebata, M. Fujii, N. Mikami, OH stretching vibrations of phenol-(H2O)n(n = 1-3) complexes observed by Ir-Uv double-resonance spectroscopy, Chem. Phys. Lett. 215 (4) (1993) 347–352.
[20] A. Sen, A. Bouchet, V. Lepère, K.L. Barbu-Debus, D. Scuderi, F. Piuzzi, A. Zehnacker-Rentien, Conformational analysis of quinine and its pseudo enantiomer quinidine: a combined jet-cooled spectroscopy and vibrational circular dichroism study, J. Phys. Chem. A 116 (32) (2012) 8334–8344.
[21] L.A. Nafie, Vibrational optical activity: from discovery and development to future challenges, Chirality 32 (5) (2020) 667–692.
[22] L.A. Nafie, Vibrational Optical Activity: Principles and Applications, John Wiley & Sons Ltd, 2011.
[23] C. Merten, T. Kowalik, A. Hartwig, Vibrational circular dichroism spectroscopy of solid polymer films: effects of sample orientation, Appl. Spectrosc. 62 (8) (2008) 901–905.
[24] T. Buffeteau, F.S. Lagugne-Labarthet, C. Sourisseau, Vibrational circular dichroism in general anisotropic thin solid films: measurement and theoretical approach, Appl. Spectrosc. 59 (6) (2005) 732–745.
[25] G.M. Sheldrick, SHELXS-97, Program for Crystal Structure Solution, University of Göttingen, Göttingen, Germany, 1997.
[26] G.M. Sheldrick, SHELXL-97, Program for the Refinement of Crystal Structures from Diffraction Data, University of Göttingen, Göttingen, Germany, 1997.
[27] L. Farrugia, WinGX suite for small-molecule single-crystal crystallography, J. Appl. Crystallogr. 32 (4) (1999) 837–838.
[28] Williams, M.J. Frisch, G.W. Trucks, H.B. Schlegel, G.E. Scuseria, M.A. Robb, J.R. Cheeseman, G. Scalmani, V. Barone, G.A. Petersson, H. Nakatsuji, X. Li, M. Caricato, A.V. Marenich, J. Bloino, B.G. Janesko, R. Gomperts, B. Mennucci, H.P. Hratchian, J.V. Ortiz, A.F. Izmaylov, J.L. Sonnenberg, F. Ding, F. Lipparini, F. Egidi, J. Goings, B. Peng, A. Petrone, T. Henderson, D. Ranasinghe, V.G. Zakrzewski, J. Gao, N. Rega, G. Zheng, W. Liang, M. Hada, M. Ehara, K. Toyota, R. Fukuda, J. Hasegawa, M. Ishida, T. Nakajima, Y. Honda, O. Kitao, H. Nakai, T. Vreven, K. Throssell, J.A. Montgomery Jr., J.E. Peralta, F. Ogliaro, M.J. Bearpark, J.J. Heyd, E.N. Brothers, K.N. Kudin, V.N. Staroverov, T.A. Keith, R. Kobayashi, J. Normand, K. Raghavachari, A.P. Rendell, J.C. Burant, S.S. Iyengar, J. Tomasi, M. Cossi, J.M. Millam, M. Klene, C. Adamo, R. Cammi, J.W. Ochterski, R.L. Martin, K. Morokuma, O. Farkas, J.B. Foresman, D.J. Fox, Gaussian 16 Rev. B.01, Wallingford, CT, 2016.
[29] M.J. Frisch, J.A. Pople, J.S. Binkley, Self-consistent molecular-orbital methods .25. Supplementary functions for Gaussian-basis sets, J. Chem. Phys. 80 (7) (1984) 3265–3269.
[30] S. Grimme, J. Antony, S. Ehrlich, H. Krieg, A consistent and accurate ab initio parametrization of density functional dispersion correction (DFT-D) for the 94 elements H-Pu, J. Chem. Phys. 132 (15) (2010) 154104.
[31] S. Grimme, S. Ehrlich, L. Goerigk, Effect of the damping function in dispersion corrected density functional theory, J. Comput. Chem. 32 (7) (2011) 1456–1465.
[32] A. Pérez Mellor, A. Zehnacker, Chirality effects in jet-cooled cyclic dipeptides, in: T. Ebata, M. Fujii (Eds.), Physical Chemistry of Cold Gas-Phase Functional Molecules and Clusters, Eds., Springer, Singapore, 2019, pp. 63–87.
[33] M.D. Halls, J. Velkovski, H.B. Schlegel, Harmonic frequency scaling factors for Hartree-Fock, S-VWN, B-LYP, B3-LYP, B3-PW91 and MP2 with the Sadlej pVTZ electric property basis set, Theor. Chem. Acc. 105 (2001) 413.
[34] A.E. Reed, L.A. Curtiss, F. Weinhold, Intermolecular interactions for a natural bond orbital, donor-acceptor viewpoint, Chem. Rev. 88 (6) (1988) 899–926.
[35] K. Hirata, Y. Mori, S.I. Ishiuchi, M. Fujii, A. Zehnacker, Chiral discrimination between tyrosine and beta-cyclodextrin revealed by cryogenic ion trap infrared spectroscopy, Phys. Chem. Chem. Phys. 22 (43) (2020) 24887–24894.
[36] S. Ishiuchi, H. Wako, D. Kato, M. Fujii, High-cooling-efficiency cryogenic quadrupole ion trap and UV-UV hole burning spectroscopy of protonated tyrosine, J. Mol. Spectrosc. 332 (2017) 45–51.
[37] J.A. Stearns, M. Guidi, O.V. Boyarkin, T.R. Rizzo, Conformation-specific infrared and ultraviolet spectroscopy of tyrosine-based protonated dipeptides, J. Chem. Phys. 127 (15) (2007) 154322.
[38] J.A. Stearns, S. Mercier, C. Seaiby, M. Guidi, O.V. Boyarkin, T.R. Rizzo, Conformation-specific Spectroscopy and photodissociation of cold, protonated tyrosine and phenylalanine, J. Am. Chem. Soc. 129 (38) (2007) 11814–11820.
[39] M. Krupova, J. Kessler, P. Bour, Recent trends in chiroptical spectroscopy: theory and applications of vibrational circular dichroism and raman optical activity, Chempluschem 85 (3) (2020) 561–575.
[40] S. Jähnigen, A. Zehnacker, R. Vuilleumier, Computation of solid-state vibrational circular dichroism in the periodic gauge, J. Phys. Chem. Lett. 12 (30) (2021) 7213–7220.
[41] S. Jähnigen, A. Scherrer, R. Vuilleumier, D. Sebastiani, Chiral crystal packing induces enhancement of vibrational circular dichroism, Angew. Chem.-Int. Edit. 57 (40) (2018) 13344–13348.
[42] R. Marty, H. Frauenrath, J. Helbing, Aggregates from perylene bisimide oligopeptides as a test case for giant vibrational circular dichroism, J. Phys. Chem. B 118 (38) (2014) 11152–11160.
[43] J.R.A. Moreno, M.M.Q. Moreno, J.J.L. Gonzalez, R.M. Claramunt, C. Lopez, I. Alkorta, J. Elguero, Self-assembly structures of 1H-indazoles in the solution and solid phases: a vibrational (IR, FIR, Raman, and VCD) spectroscopy and computational study, ChemPhysChem 14 (14) (2013) 3355–3360.
[44] J.J.L. Gonzalez, F.P. Urena, J.R.A. Moreno, I. Mata, E. Molins, R.M. Claramunt, C. Lopez, I. Alkorta, J. Elguero, The chiral structure of 1H-indazoles in the solid state: a crystallographic, vibrational circular dichroism and computational study, N. J. Chem. 36 (3) (2012) 749–758.

[45] J.R. Cheeseman, M.J. Frisch, F.J. Devlin, P.J. Stephens, Ab initio calculation of atomic axial tensors and vibrational rotational strengths using density functional theory, Chem. Phys. Lett. 252 (3–4) (1996) 211–220.
[46] P.J. Stephens, Theory of vibrational circular-dichroism, J. Phys. Chem. 89 (5) (1985) 748–752.
[47] J. Contreras-Garcia, E.R. Johnson, S. Keinan, R. Chaudret, J.P. Piquemal, D.N. Beratan, W.T. Yang, NCIPLOT: a program for plotting noncovalent interaction regions, J. Chem. Theory Comput. 7 (3) (2011) 625–632.
[48] R. Chaudret, B.d. Courcy, J. Contreras-Garcia, E. Gloaguen, A. Zehnacker-Rentien, M. Mons, J.P. Piquemal, Unraveling non covalent interactions within flexible biomolecules: from electron density topology to gas phase spectroscopy, Phys. Chem. Chem. Phys. 16 (2014) 9876–9891.
[49] M. Jackson, H.H. Mantsch, Beware of proteins in DMSO, Biochim. Biophys. Acta 1078 (2) (1991) 231–235.
[50] I. Alata, A. Pérez-Mellor, F. Ben Nasr, D. Scuderi, V. Steinmetz, F. Gobert, N.E. Jaïdane, A. Zehnacker-Rentien, Does the residues chirality modify the conformation of a cyclo-dipeptide? Vibrational spectroscopy of protonated cyclo-diphenylalanine in the gas phase, J. Phys. Chem. A 121 (38) (2017) 7130–7138.
[51] A. Pérez-Mellor, K.L. Barbu-Debus, V. Lepere, I. Alata, R. Spezia, A. Zehnacker, Structure and collision-induced dissociation of the protonated cyclo His-Phe dipeptide: mechanistic studies and stereochemical effects, Eur. Phys. J. D 75 (6) (2021).
[52] M. Alauddin, E. Gloaguen, V. Brenner, B. Tardivel, M. Mons, A. Zehnacker-Rentien, V. Declerck, D.J. Aitken, Intrinsic folding proclivities in cyclic -peptide building blocks: configuration and heteroatom effects analyzed by conformer-selective spectroscopy and quantum chemistry, Chem. Eur. J. 21 (46) (2015) 16479–16493.
[53] P.R. Shirhatti, S. Wategaonkar, Mass analyzed threshold ionization (MATI) spectroscopy of p-cresol, Indian J. Phys. 86 (3) (2012) 159–164.
[54] K.T. Lu, G.C. Eiden, J.C. Weisshaar, Toluene cation - nearly free rotation of the methyl-group, J. Phys. Chem. 96 (24) (1992) 9742–9748.
[55] S.J. Martinez, J.C. Alfano, D.H. Levy, The electronic spectroscopy of the amino-acids tyrosine and phenylalanine in a supersonic jet, J. Mol. Spectrosc. 156 (2) (1992) 421–430.
[56] Y. Inokuchi, Y. Kobayashi, T. Ito, T. Ebata, Conformation of L-tyrosine studied by fluorescence-detected UV-UV and IR-UV double-resonance spectroscopy, J. Phys. Chem. A 111 (17) (2007) 3209–3215.
[57] Y. Shimozono, K. Yamada, S. Ishiuchi, K. Tsukiyama, M. Fujii, Revised conformational assignments and conformational evolution of tyrosine by laser desorption supersonic jet laser spectroscopy, Phys. Chem. Chem. Phys. 15 (14) (2013) 5163–5175.
[58] L.C. Snoek, E.G. Robertson, R.T. Kroemer, J.P. Simons, Conformational landscapes in amino acids: infrared and ultraviolet ion-dip spectroscopy of phenylalanine in the gas phase, Chem. Phys. Lett. 321 (1–2) (2000) 49–56.
[59] T. Hashimoto, Y. Takasu, Y. Yamada, T. Ebata, Anomalous conformer dependent S-1 lifetime of L-phenylalanine, Chem. Phys. Lett. 421 (1–3) (2006) 227–231.
[60] I.K. Chu, C.F. Rodriguez, F. Rodriguez, A.C. Hopkinson, K.W.M. Siu, Formation of molecular radical cations of enkephalin derivatives via collision-induced dissociation of electrospray-generated copper (II) complex ions of amines and peptides, J. Am. Soc. Mass Spectrom. 12 (10) (2001) 1114–1119.
[61] J. Szafranek, Z. Palacz, Z. Grzonka, Comparison of electron-impact and field-ionization spectra of some 2,5-diketopiperazines, Org. Mass Spectrom. 11 (9) (1976) 920–930.
[62] E. Fujimaki, A. Fujii, T. Ebata, N. Mikami, Autoionization-detected infrared spectroscopy of intramolecular hydrogen bonds in aromatic cations. I. Principle and application to fluorophenol and methoxyphenol, J. Chem. Phys. 110 (9) (1999) 4238–4247.
[63] E. Gloaguen, M. Mons, K. Schwing, M. Gerhards, Neutral peptides in the gas phase: conformation and aggregation issues, Chem. Rev. 120 (22) (2020) 12490–12562.
[64] M. Gdaniec, B. Liberek, Structure of cyclo(-L-phenylalanyl-L-phenylalanyl-), Acta Crystallogr. Sect. C-Cryst. Struct. Commun. 42 (1986) 1343–1345.
[65] T. Taniguchi, K. Monde, Exciton chirality method in vibrational circular dichroism, J. Am. Chem. Soc. 134 (8) (2012) 3695–3698.
[66] K. Bünnemann, C. Merten, Solvation of a chiral carboxylic acid: effects of hydrogen bonding on the IR and VCD spectra of [small alpha]-methoxyphenylacetic acid, Phys. Chem. Chem. Phys. 19 (29) (2017) 18948–18956.
[67] K. Le Barbu-Debus, A. Zehnacker, Competition between inter and intramolecular hydrogen bond evidenced by vibrational circular dichroism spectroscopy: the case of (1S,2R)-(-)-cis-1-amino-2-indanol, Chirality 33 (12) (2021) 858–874.
[68] K. Le Barbu-Debus, J. Bowles, S. Jähnigen, C. Clavaguéra, F. Calvo, R. Vuilleumier, A. Zehnacker, Assessing cluster models of solvation for the description of vibrational circular dichroism spectra: synergy between static and dynamic approaches, Phys. Chem. Chem. Phys. 22 (45) (2020) 26047–26068.